WPS1-CPR(18) 19426

T Estrada et al.

Turbulence and radial electric field asymmetries measured at TJ-II plasmas

Preprint of Paper to be submitted for publication in Proceeding of
27th IAEA Fusion Energy Conference

This work has been carried out within the framework of the EUROfusion Consortium and has received funding from the Euratom research and training programme 2014-2018 under grant agreement No 633053. The views and opinions expressed herein do not necessarily reflect those of the European Commission.

Turbulence and radial electric field asymmetries measured at TJ-II plasmas

T Estrada[1], E. Sánchez[1], J.M. García-Regaña[1], J.A. Alonso[1], E. Ascasíbar[1], I. Calvo[1], A. Cappa[1], D. Carralero[1], C. Hidalgo[1], M. Liniers[1], I. Pastor[1], J.L. Velasco[1], and the TJ-II team[1]

[1] Laboratorio Nacional de Fusión. CIEMAT, 28040 Madrid, Spain

E-mail: teresa.estrada@ciemat.es

Abstract.

Dedicated experiments have been carried out for a systematic comparison of turbulence wavenumber spectra and perpendicular rotation velocity measured at poloidally separated positions in the same flux-surface in the stellarator TJ-II. The rationale behind this study is twofold, verification of the spatial localization of instabilities predicted by the gyrokinetic simulations in stellarators and verification of the electrostatic potential variation on the flux surface as calculated by neoclassical codes and its possible impact on the radial electric field. Perpendicular wavenumber spectra and perpendicular rotation velocity profiles have been measured using Doppler reflectometry in two plasma regions poloidally separated as both positive and negative probing beam angles with respect to normal incidence can be selected. A systematic comparison has been carried out showing differences in the perpendicular wavenumber spectrum measured at poloidally separated positions in the same flux-surface, that depend on plasma density, heating conditions and magnetic configuration. The asymmetry found in the standard magnetic configuration under some plasmas conditions, reverses in the high iota configuration. The different intensity in the density fluctuation spectra can be related to the poloidal localization of instabilities found in the gyrokinetic simulations. Differences in the radial electric field profile are also found that could be explained to be due to plasma potential variations within the flux surfaces.

PACS numbers: 52.70.Gw, 52.55.-s, 52.35.Bj, 52.35.Ra

1. Introduction

The transport of energy and particles in magnetically confined fusion plasmas can be largely determined by turbulence in the plasma gradient region [1]. The appropriate framework to study plasma turbulence is the gyrokinetic formalism, which makes kinetic simulations with codes based on it affordable. However, these codes should be carefully validated against experiment in order to be useful for actual prediction. Scale resolved turbulence measurements are important in order to identify the type of turbulence and for the validation of turbulence simulations. In stellarators, gyrokinetic simulations

show a distribution of the turbulence fluctuations on the magnetic surfaces that differs from that in tokamaks [2–5]. The geometric properties of the field lines vary greatly over the magnetic surfaces and unstable modes have the maximum amplitude in locations of bad magnetic field line curvature and small local magnetic shear. In TJ-II, gyrokinetic simulations show that the electrostatic instabilities (ITG, TEM and ETG) are localized in narrow stripes along certain magnetic field lines [6]. The predicted localization of instabilities has motivated a number of experiments in TJ-II for a systematic comparison of the perpendicular wavenumber spectra measured at two poloidally separated positions using Doppler reflectometry.

On the other hand, in stellarators, it is the neoclassical transport that determines the electric field. In most cases, neoclassical calculations only consider the lowest order electrostatic potential that only depends on the flux surface label, and gives the radial electric field. However, variations of the neoclassical electrostatic potential over the flux surface, so called φ_1, can be relatively large under certain plasma conditions, namely at low collisionalities, giving electric fields tangential to the flux surface [7, 8]. At TJ-II, observations of potential variations along the flux surfaces, measured using two distant Langmuir probe arrays, have been previously reported [9]. Differences in the edge floating potentials profiles of several tens of volts were measured in low density plasmas in agreement with the overall variation in potential obtained in the neoclassical simulations. The relevance of the electrostatic potential variation on the flux surface, φ_1, lies in its effect on the neoclassical impurity transport [10–12]. In addition, φ_1 may impact the local radial electric field through its radial variation. This possible impact has been studied in this work by the comparison between the perpendicular rotation velocity of the plasma turbulence, that in general it is dominated by the $E \times B$ velocity, measured at two poloidally separated positions using Doppler reflectometry.

Doppler Reflectometry makes use of a finite tilt angle between the probing beam and the cut-off layer normal to measure the Bragg back-scattered process that takes place at the cut-off layer. This technique allows the measurement of the density turbulence and its perpendicular rotation velocity, at different turbulence scales and with good spatial and temporal resolution [13–18]. In particular, the Doppler Reflectometer (DR) in operation at TJ-II allows measuring at two plasma regions poloidally separated [16].

Dedicated experiments have been carried out in different plasma scenarios for a systematic comparison of the Doppler reflectometer measurements −perpendicular wavenumber spectrum and radial electric field− at poloidally separated positions in the same flux-surface. This paper focusses on the description of these experimental results and how they compare with numerical simulations which are either recently reported or still under study.

The remainder of the paper is organized as follows. The Doppler reflectometer measurement capabilities are described in section 2 and the experimental results in section 3: those related to the perpendicular wavenumber spectra in section 3.1 and those describing the radial electric field in section 3.2. Finally, a discussion and the summary are included in sections 4 and 5, respectively.

2. Experimental set-up

TJ-II is a helical device with major radius $R = 1.5$ m, minor radius $a \leq 0.22$ m and magnetic field $B_0 \leq 1.2$ T. TJ-II offers the possibility to explore a wide rotational transform range in low, negative magnetic shear configurations. Plasmas are created and heated by Electron Cyclotron Heating (ECH) 2^{nd} harmonic using two gyrotrons at 53.2 GHz with X-mode polarization. The maximum power per gyrotron is 300 kW and the power deposition profile can be changed from on-axis to off-axis heating conditions, by moving the last mirror of the two ECH quasi-optical transmission lines. These mirrors, located inside the vacuum vessel, are steerable in both poloidal and toroidal angles [19]. Under ECH heating conditions the plasma density has to be kept below the cut-off value of 1.75×10^{19} m^{-3}. Higher density plasmas are achieved using Neutral Beam Injection (NBI) heating. Two injectors, one co- and one counter-, are in operation delivering a port-through power per injector up to 700 kW [20].

Doppler Reflectometry is used to measure the density turbulence and its perpendicular rotation velocity, at different turbulence scales and with good spatial and temporal resolution [13–18]. In TJ-II, an optimized Doppler Reflectometer (DR) is in operation since 2009 [16]. The reflectometer works in a frequency hopping mode in the Q-band: $33 - 50$ GHz, covering typically the radial region from $\rho \sim 0.6$ to 0.9, ρ being the normalized effective radius. Its in-vessel front-end consist of a compact corrugated antenna and an ellipsoidal mirror that focus the probing microwave beam to the cut-off layer with a well defined optimized beam waist. The mirror can be tilted to probe different perpendicular wave-numbers of the turbulence, covering the range: $k_\perp = 1 - 14$ cm^{-1}. This $k_\perp - \rho$ parameter range can be explored in two plasma regions poloidally separated as illustrated in figure 1.left. In the following, the region on the left of the plasma cross section shown in the figure will be called *region_1* and that on the right *region_2*. The $k_\perp$ and ρ values in each particular scenario are calculated using the ray-tracing code TRUBA [21], that takes into account the propagation of the microwave beam in the three dimensional structure of the TJ-II magnetic configuration and the corresponding density profile. An example of the $k_\perp - \rho$ parameter range explored in the two poloidal plasma regions is shown in figure 1.right.

The perpendicular rotation velocity of the plasma turbulence measured by Doppler reflectometry is a composition of both the plasma $E \times B$ velocity and the intrinsic phase velocity of the density fluctuations: $u_\perp = v_{E\times B} + v_{ph}$. In cases in which the condition $v_{E\times B} >> v_{ph}$ holds, the radial electric field can be obtained directly from the perpendicular rotation velocity: $E_r = u_\perp B$ [22]. In TJ-II, previous measurements carried out in ECH and NBI plasmas support the conclusion that $v_{E\times B} >> v_{ph}$ allowing, in these cases, the determination of E_r [17].

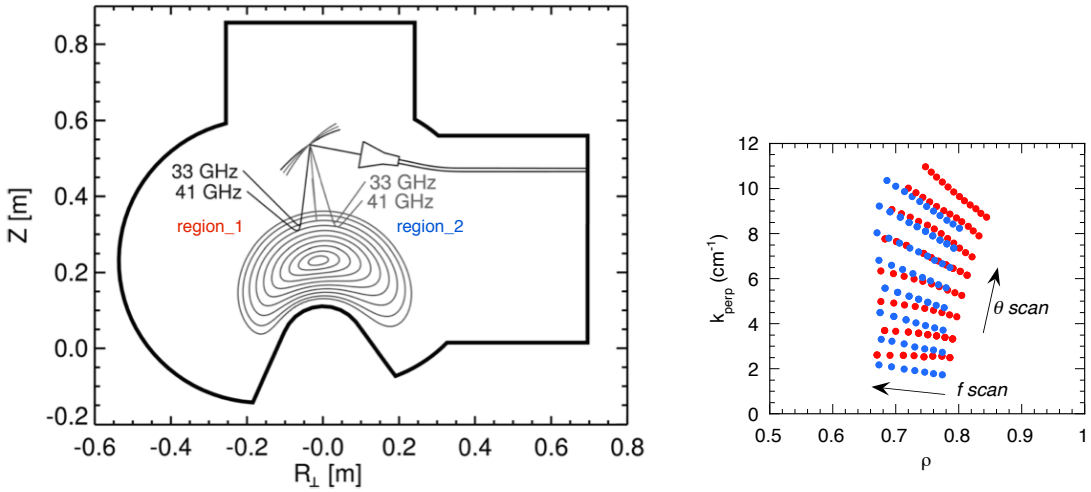

Figure 1. Left: schematic representation of the TJ-II vacuum vessel with the DR antenna-mirror arrangement showing the two poloidally separated plasma regions that can be probed by the system. Right: example of the $k_\perp - \rho$ parameter range explored in the two plasma regions.

3. Experimental results

3.1. Perpendicular wavenumber spectra

A set of experiments with the goal of characterizing the turbulence under different regimes in TJ-II have been carried out during the last TJ-II campaigns. Different plasma scenarios have been studied with different plasma profile shapes, namely, high power on-axis ECH heated plasmas vs. low power off-axis ECH heated plasmas; ECH vs. NBI heated plasmas; standard vs. high rotational transform magnetic configurations; Hydrogen vs. Deuterium dominated plasmas. The electron temperature and density profiles obtained applying a Bayesian analysis [23] to the experimental data obtained using microwave interferometry, Thomson scattering [24], AM reflectometry [25], He-beam [26] and ECE [27], in a representative discharge of each series, are depicted in figure 2.a−2.e. In these experiments only the ion temperature along a central plasma chord was measured by CX-NPA [28]. However, as reported in [29], rather flat T_i profiles are expected. In all cases scale-resolved density fluctuation spectra have been measured at different radial positions and in the two poloidally separated plasma regions.

3.1.1. Standard magnetic configuration. As first scenario, on-axis ECH-heated low-density plasma (with $n_e = 0.5 \times 10^{19}$ m^{-3} and $P_{ECH} = 500$ kW) in the standard magnetic configuration (rotational transform at the plasma edge: $\iota_a = 1.63$), is selected. The electron temperature and density profiles are shown in figure 2.a. The central electron and ion temperature are respectively $T_e(0) = 1.5$ keV and $T_i(0) = 100$ eV. In each discharge the DR probing frequencies are changed to probe different radial positions while the probing beam angle is scanned in a shot to shot basis. As already mentioned, ρ and $k_\perp$ are calculated for each probing frequency and beam angle, using the ray-tracing

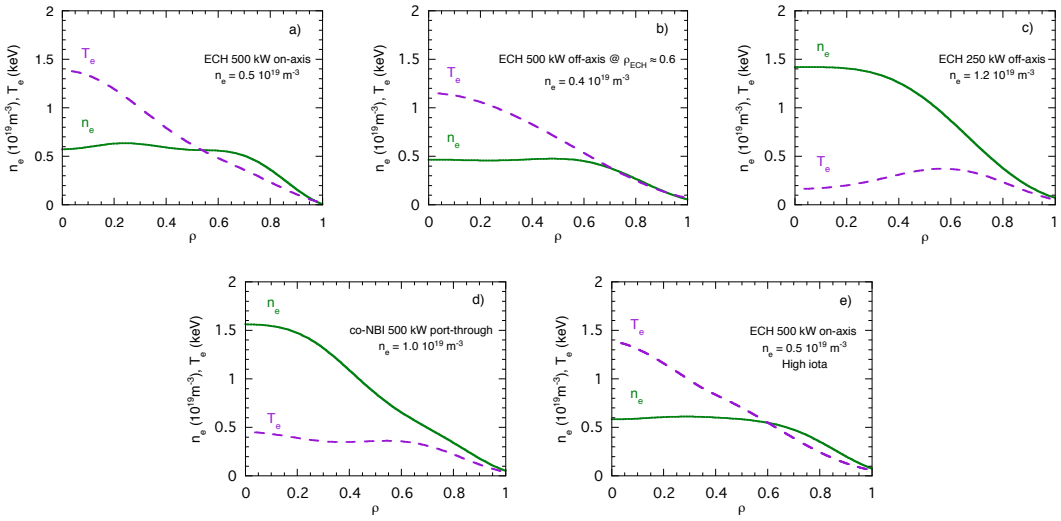

Figure 2. Electron temperature and density profiles obtained applying a Bayesian analysis to the experimental data obtained in the different plasma scenarios.

code TRUBA with the density profile representative of the series (shown in figure 2.a).

The perpendicular wavenumber spectra measured by the DR in the two poloidally separated plasma regions are shown in figure 3 (*region_1* left in red and *region_2* right in blue). The spectra are measured at $\rho = 0.78 \pm 0.04$ (figure 3.a) and at $\rho = 0.69 \pm 0.04$ (figure 3.b), respectively. An asymmetry is clearly observed in the intensity of the density fluctuations in the whole $k_\perp$ range. Higher turbulence level is measured in *region_1* as compared with that measured in *region_2*, being the difference more pronounced in the outer radial position, i.e. at $\rho = 0.78 \pm 0.04$, and at intermediate turbulence scales, i.e. $k_\perp \sim 4 - 7$ cm^{-1} (figure 3.a). At the inner radial position the turbulence level measured in *region_1* decreases getting closer to the level measured in *region_2* (figure 3.b). This result is consistent with a turbulence drive radially localized closer to the outer position of measurement and asymmetrically distributed over the magnetic surface.

The poloidal asymmetry discovered in the first scenario is not found when comparing the perpendicular wavenumber spectra measured in low density ECH plasmas in which the ECH power is deposited off-axis at $\rho_{ECH} = 0.64$. In this second scenario, the electron temperature profile is rather flat with $T_e(0) = 1.0$ keV, and $T_i(0) = 75$ eV. The electron temperature and density profiles are shown in figure 2.b.The perpendicular wavenumber spectra measured in the radial range $\rho = 0.6 - 0.8$ are shown in figure 4. Very similar density turbulence level is measured in the two poloidal regions and in the covered radial range.

In order to compare with these experimental results, global gyrokinetic simulations using the code EUTERPE [3, 30] are being performed [6, 31]. Linear analyses of instabilities have been done considering kinetic ions and electrons, collisions, and experimental density, temperature and radial electric field profiles. The instabilities are driven by the electron temperature gradient and the main contribution comes from the

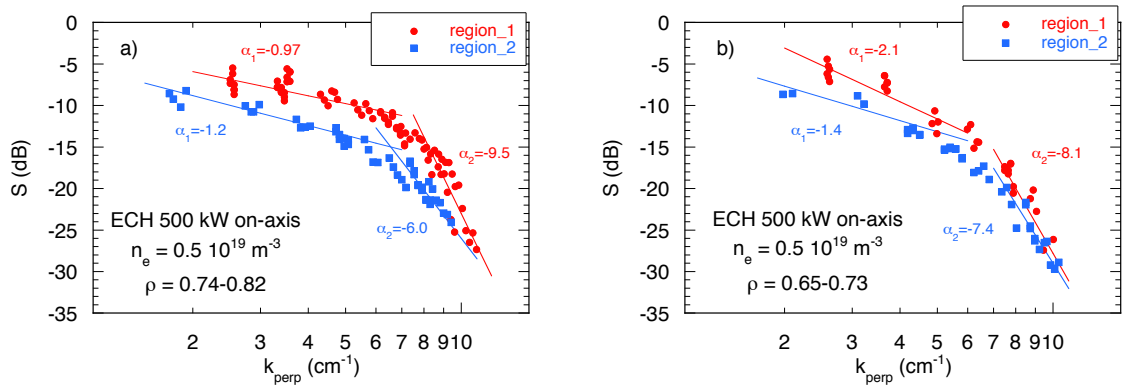

Figure 3. $k_\perp$ spectra measured by the DR in the two plasma regions poloidally separated (*region_1* in red and *region_2* in blue) at $\rho = 0.78 \pm 0.04$ (a) and at $\rho = 0.69 \pm 0.04$ (b). $P_{ECH} = 500$ kW on-axis, $n_e = 0.5\ 10^{19}$ m^{-3}, standard magnetic configuration.

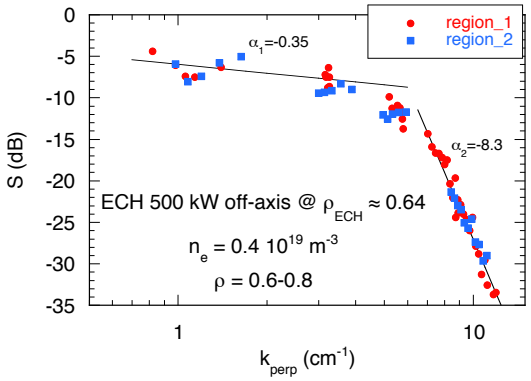

Figure 4. $k_\perp$ spectra measured by the DR in the two plasma regions poloidally separated (*region_1* in red and *region_2* in blue) at $\rho = 0.7 \pm 0.1$. $P_{ECH} = 500$ kW off-axis at $\rho_{ECH} = 0.64$, $n_e = 0.4\ 10^{19}$ m^{-3}, standard magnetic configuration.

∇B term, compatible with Trapped Electron Modes (TEM). Differences in the radial localization of the most unstable modes are found when comparing the two plasma scenarios. In the first scenario these modes are located at $\rho \sim 0.75 - 0.95$, while in the second scenario the modes are located at inner radial positions $\rho \sim 0.65 - 0.85$. The outer localization of the instable modes in the first scenario may be consistent with the radial dependence found in the experiments, particularly in *region_1* where higher turbulence levels are detected. Regarding the turbulence localization along the flux surface, an asymmetry is also observed in the simulations, however, a quantitative agreement with the experiments has not been found yet. Non-linear simulations are in progress to proceed with the simulation/experiment comparisons.

A third scenario with higher density plasmas ($n_e = 1.2{\times}10^{19}$ m^{-3}) heated with lower ECH power ($P_{ECH} = 250$ kW) deposited off-axis at $\rho_{ECH} = 0.4$, has been also explored. Under this conditions, $T_i(0) = 90$ eV and lower electron temperatures are measured with

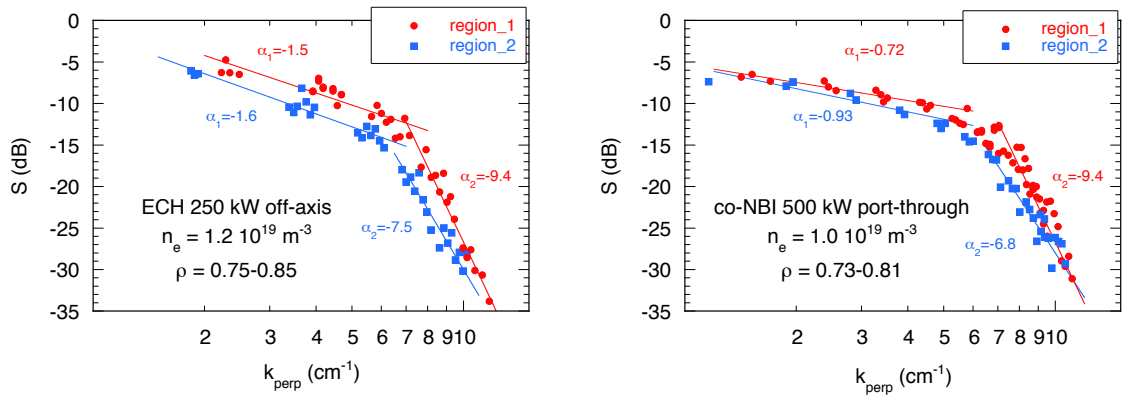

Figure 5. $k_\perp$ spectra measured by the DR in the two plasma regions poloidally separated (*region*_1 in red and *region*_2 in blue) at (left) $\rho = 0.80 \pm 0.05$ in ECH high density plasmas with $P_{ECH} = 250$ kW off-axis at $\rho_{ECH} = 0.4$ and $n_e = 1.2\ 10^{19}$ m^{-3}, and (right) at $\rho = 0.77 \pm 0.04$ in pure NBI heated plasmas $P_{NBI} = 500$ kW port-through, $n_e = 1.0\ 10^{19}$ m^{-3}, both in the standard magnetic configuration.

hollow profiles (see figure 2.c). In these plasmas the collisionality is higher than in the previous scenarios and the radial electric field is negative in the whole plasma column, i.e. the plasma is in the neoclassical ion root confinement regime. A poloidal asymmetry in the perpendicular wavenumber spectra is found with a behaviour that resembles that found in the first scenario, i.e., higher turbulence level in *region*_1 as compared with *region*_2 (see figure 5.left). This scenario, however, presents a particular behaviour regarding the perpendicular rotation velocity and its dependence on the turbulence scale. This point will be discussed in section 3.2.

Similar plasma parameters as those in the third scenario are measured when heating with only NBI at moderate plasma densities ($n_e = 1.0 \times 10^{19}$ m^{-3}). With a port-through power of $P_{NBI} = 500$ kW, flat temperature profiles are measured with $T_e(0) = 0.4$ keV, and $T_i(0) = 120$ eV. The electron temperature and density profiles are shown in figure 2.d. This fourth scenario has been also investigated searching for poloidal asymmetries in the plasma turbulence. As in the first and third scenarios, higher turbulence level is measured in *region*_1 as compared with *region*_2. The perpendicular wavenumber spectra measured in these plasmas in the radial range $\rho = 0.73 - 0.81$ are shown in figure 5.right. Although less pronounced than in the first and third scenarios, a difference in the turbulence level at intermediate turbulence scales is clearly visible.

3.1.2. Magnetic configuration with high rotational transform. A magnetic configuration with higher rotational transform ($\iota_a = 2.24$) has been studied under the same experimental conditions as in the first scenario: on-axis ECH-heated low-density plasma (with $n_e = 0.5 \times 10^{19}$ m^{-3} and $P_{ECH} = 500$ kW). As for the first scenario in the standard magnetic configuration, the electron temperature profile is peaked with central values of $T_e(0) = 1.5$ keV, and $T_i(0) = 100$ eV. The electron temperature and density profiles are shown in figure 2.e. The perpendicular wavenumber spectra measured in the two

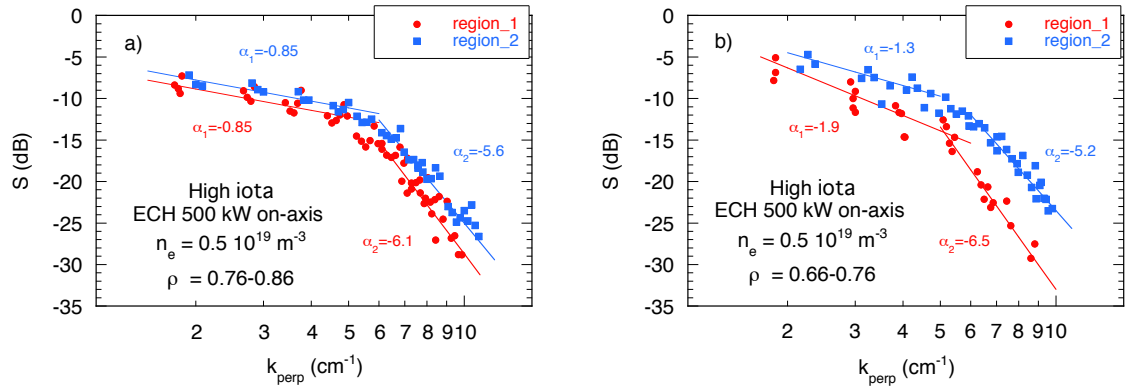

Figure 6. $k_\perp$ spectra measured by the DR in the two plasma regions poloidally separated (*region_1* in red and *region_2* in blue) at $\rho = 0.81 \pm 0.05$ (a) and at $\rho = 0.71 \pm 0.05$ (b). $P_{ECH} = 500$ kW on-axis, $n_e = 0.5\ 10^{19}$ m^{-3}, magnetic configuration with high rotational transform.

poloidally separated plasma regions are shown in figure 6. The spectra in this high ι configuration are measured at $\rho = 0.81 \pm 0.05$ (figure 6.a) and at $\rho = 0.71 \pm 0.05$ (figure 6.b), and as in the standard magnetic configuration, a poloidal asymmetry in the perpendicular wavenumber spectra is found. However in this magnetic configuration, the fluctuation level is higher in *region_2* as compared with *region_1*, and the poloidal asymmetry is more pronounced at the inner radial region. It is worth mentioning that, as for the data recorder so far, this reversal in the poloidal asymmetry is specific of this magnetic configuration with high rotational transform.

The influence of the rotational transform on the turbulence localization along the flux surface has been also studied by gyrokinetic simulations [31]. The maximum amplitude of the instabilities is displaced poloidally when the rotational transform is increased as observed in the experiments. However, a quantitative agreement with the experiments has not been found yet.

3.1.3. Influence of isotope mass. Recently, the influence of isotope mass has been investigated in TJ-II finding similarities in Hydrogen and Deuterium dominated plasmas during the L-H transition in NBI plasma scenarios [32]. In general, similar density, temperature and E_r profiles are obtained in Hydrogen and Deuterium plasmas, when the same heating conditions and magnetic configuration are considered. The influence of the isotope mass on the turbulence wavenumber spectrum has been also studied both in ECH and NBI plasmas. In the first case, pure Hydrogen and Deuterium plasmas heated with on-axis ECH at low-density (with $n_e = 0.5 \times 10^{19}$ m^{-3} and $P_{ECH} = 500$ kW) are compared. In the second case, pure Hydrogen and Deuterium dominated plasmas (up to 70%) heated with NBI at moderate density (with $n_e = 1.0 \times 10^{19}$ m^{-3} and $P_{NBI} = 500$ kW) are considered. The heating scenario (ECRH vs NBI) induces a change in the wavenumber spectra −the turbulence level is higher in ECRH than in NBI plasmas− however, the isotope mass does not affect the properties of the turbulence,

neither the amplitude nor the spectral shape or the poloidal asymmetry, in either of the two heating scenarios. The insensitivity of the turbulence spectrum to the ion mass found in the experiments has been compared with simulations. As the unstable modes are mainly driven by electrons in these plasma conditions, a weak dependence of spectra on ion mass is expected. In fact, global gyrokinetic simulations performed for the ECH-heated plasmas show that the spectra of the linearly unstable modes in Hydrogen and Deuterium plasmas are very similar, in good agreement with the experimental results.

3.1.4. Shape of the $k_\perp$ spectrum. The $k_\perp$ spectra measured in the present experiments show a density turbulence level that decreases from large towards small scales. In general, two separate $k_\perp$ regions are identified that can be characterized by a power law behavior with different spectral indices, α_1 and α_2, as shown in figures 3−6. At large scales, $k_\perp \lesssim 5$ cm^{-1}, a slight dependence of the turbulence level on the wavenumber is measured with a spectral index α_1 in the range from -0.5 to -2. At small scales, $k_\perp \gtrsim 7$ cm^{-1}, the turbulence level dependence on the wavenumber is stronger with α_2 in the range from -5 to -10. In between the two $k_\perp$ ranges, commonly named inertial ranges [33], a knee can be identified at $k_\perp \sim 6-7$ cm^{-1} representing the scale at which the energy is injected into the system. This turbulence scale corresponds to a normalized wavenumber $k_\perp \rho_s \sim 1.2$, where $\rho_s = \sqrt{2m_i T_e}/eB$ is the ion Larmor radius evaluated at electron temperature. The range of injection scales found in the experiments is congruent with the gyrokinetic simulations in which the instabilities driven by the electron temperature gradient are compatible with TEM whose most unstable modes are found at $k_\perp \sim 5-9$ cm^{-1} [31].

The spectral indices measured in different plasmas scenarios at the two inertial ranges are plotted in figure 7. As for the turbulence level, a strong poloidal asymmetry is found in the spectral index but mainly at small scales (α_2). A more pronounced spectral decay is measured in *region_1* as compared to *region_2*. At large scales, however, almost no poloidal asymmetries in the spectral index α_1 are measured. Regarding the injection scale, no systematic differences are found when comparing the $k_\perp$ spectra measured in the two poloidal plasma regions. It is worth mentioning that the shape of the wavenumber spectra measured by Doppler reflectometry may be affected by some instrumental effects, however, as discussed in section 4, these effects do not change the main conclusions regarding the poloidal asymmetries.

3.2. Radial electric field

Different plasma conditions have been explored searching for poloidal asymmetries in the radial electric field measured by DR. The most pronounced poloidal asymmetries are found in low density plasmas in the neoclassical electron root confinement regime. In TJ-II, the transition from the electron to the ion root takes place when the density exceeds some critical value that depends on the heating power and plasma volume [34]. Below the critical density, E_r is positive in the whole plasma column, and as the density

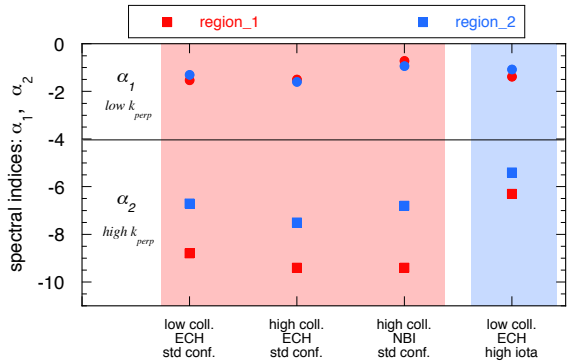

Figure 7. Spectral indices measured at low and high $k_\perp$ ranges: $k_\perp \lesssim 5$ cm^{-1} and $k_\perp \gtrsim 7$ cm^{-1}, respectively; in the different plasma scenarios, and in the two poloidal plasma regions. The colored areas delimit the scenarios at which the turbulence level is higher in *region_1* than in *region_2* (red) and viceversa (blue).

approaches the critical value, the inversion in E_r is observed; the inversion starts in the region of maximum density gradient and expands radially in agreement with neoclassical calculations [35, 36]. The perpendicular rotation velocity measured at the two poloidal regions shows pronounced differences in low density plasmas, i.e. in neoclassical electron root confinement regime. An example is shown in figure 8. The $u_\perp$ profiles measured at turbulence scales in the range $k_\perp \sim 6 - 8$ cm^{-1}, in the two poloidal plasma regions (*region_1* in red and *region_2* in blue) for plasmas in electron and ion root confinement regimes are shown together with the corresponding electron density profiles. At low densities, a pronounced poloidal asymmetry is found in the rotation velocity over the radial range $\rho \sim 0.6 - 0.8$. Under the same heating conditions, a slight increase in the density produces the inversion in $u_\perp$. In this case, the poloidal asymmetry in $u_\perp$ is lost and the profiles measured in the two poloidal plasma regions overlap to each other (open symbols in figure 8.left). The poloidal asymmetry in $u_\perp$ in the electron root confinement regime is found both in Hydrogen and Deuterium plasmas, in the standard magnetic configuration. Besides, as it will be shown later, similar values of $u_\perp$ are found in the magnetic configuration with high rotational transform for the same heating conditions. However, as for the turbulence level, the asymmetry in $u_\perp$ reverses and $u_\perp$ in *region_1* is higher than $u_\perp$ in *region_2*.

Assuming that $u_\perp$ is dominated by the $v_{E\times B}$, i.e. that the intrinsic phase velocity of the turbulence is negligible, the asymmetry in $u_\perp$ found in the electron root confinement regime in the standard magnetic configuration yields differences in E_r of about 1 kV/m ($E_r = u_\perp B$, with $B \approx 0.9$ T). Two experimental observations support the assumption $v_{E\times B} >> v_{ph}$ in these plasma conditions: on the one hand, the good agreement between the E_r profiles measured using HIBP and DR in low density electron root plasmas [6,17], and on the other hand, the lack of dependence of $u_\perp$ on the turbulence scale, $k_\perp$. The later is illustrated in figure 9. It shows the perpendicular rotation velocity plotted as a function of ρ (figure 9.a) and as a function of $k_\perp$ (figure 9.b). The data was

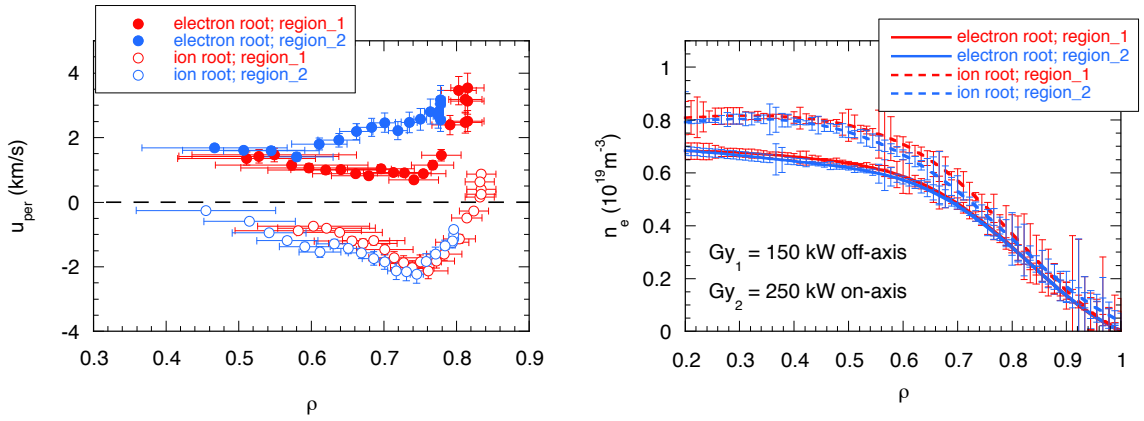

Figure 8. Left: $u_\perp$ profiles measured by the DR at turbulence scales in the range $k_\perp \sim 6-8$ cm^{-1}, in the two plasma regions poloidally separated (*region_1* in red and *region_2* in blue) in both electron and ion root regimes. Right: density profiles measured in the corresponding discharges. The experiments are performed in ECH plasmas (with gyrotron 2 at 250 kW on-axis and gyrotron 1 at 150 kW off-axis), in the standard magnetic configuration.

measured in the first scenario described in section 3.1.1. $u_\perp$ increases radially in the two poloidal plasma regions and no clear trend is found in the $u_\perp$ vs. $k_\perp$ representation, indicating that all turbulence scales propagate at the same velocity that only depends on the radial and poloidal position. This result allows us to conclude that the intrinsic phase velocity of the plasma turbulence, that naturally depends on $k_\perp$ via the dispersion relation, should be negligible as compared with $v_{E\times B}$. As it will be shown below, this behaviour is not observed for some specific plasma conditions and therefore it cannot be generalized.

The rather large poloidal asymmetry in E_r found experimentally in the electron root regime as well as the lack of asymmetry found in the ion root regime (figure 8.left), motivated the numerical analysis of the radial electric field taking into account the contribution arising from the radial dependence of the neoclassical electrostatic potential variation on the flux surfaces: $-\varphi_1'$. For the analysis, the neoclassical version of the code EUTERPE was used taking into account the experimental plasma profiles [37]. The results showed variations in E_r comparable to those found in the experiments. The contribution from the neoclassical electrostatic potential varying within the flux surfaces, $-\varphi_1'$, introduces an asymmetry in the local E_r that is a significant fraction of the ambipolar E_r in the electron root regime and much smaller in the ion root regime. It should be mentioned, however, a disagreement regarding the sign of the E_r correction when simulations and experiments are compared. Future simulations are planed to study the effect of the tangential magnetic drift on φ_1. This has been demonstrated to be very relevant under some plasma conditions, affecting not only the strength but also the phase of φ_1 [38].

As already pointed out, $u_\perp$ profiles have been also measured in the magnetic configuration with high rotational transform. As for the $k_\perp$ spectra case, a reversal in

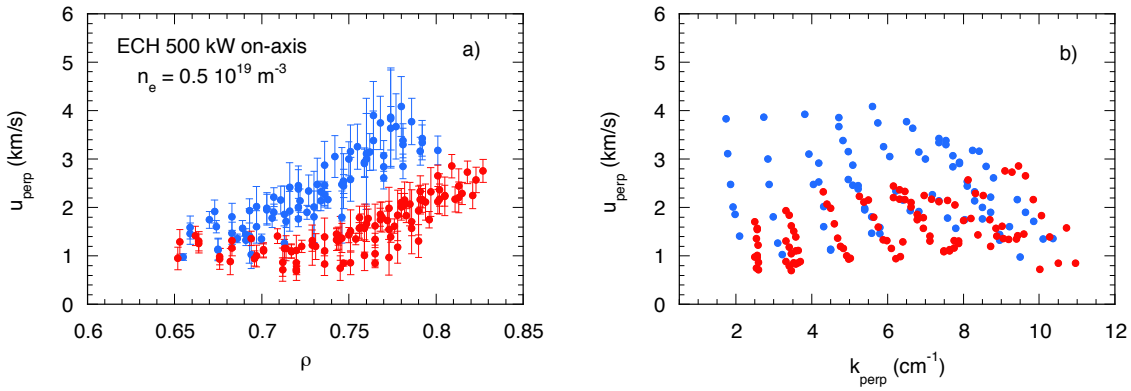

Figure 9. $u_\perp$ measured by the DR in the two poloidal regions (*region_1* in red and *region_2* in blue) in the electron root regime, as a function of ρ (a) and $k_\perp$ (b). $P_{ECH} = 500$ kW on-axis, $n_e = 0.5\ 10^{19}$ m^{-3}, standard magnetic configuration..

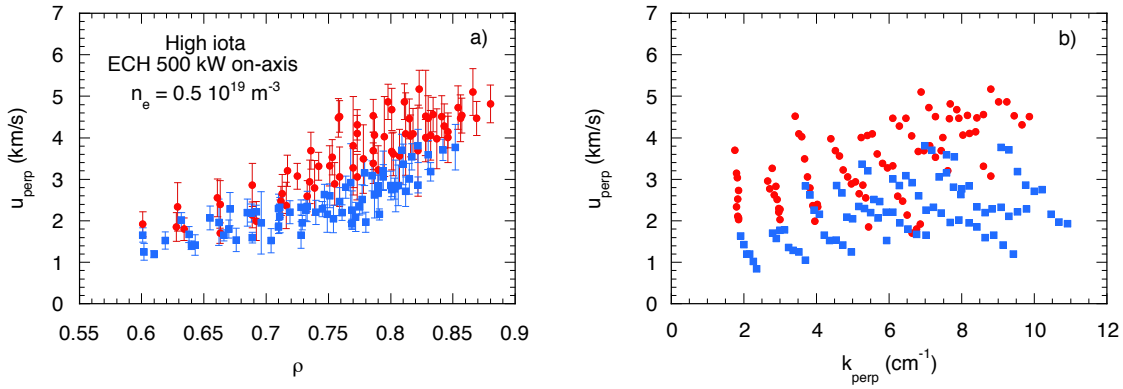

Figure 10. $u_\perp$ measured by the DR in the two poloidal regions (*region_1* in red and *region_2* in blue) in the electron root regime, as a function of ρ (a) and $k_\perp$ (b). $P_{ECH} = 500$ kW on-axis, $n_e = 0.5\ 10^{19}$ m^{-3}, magnetic configuration with high rotational transform.

the behaviour of $u_\perp$ is found when comparing the profiles measured at the two poloidal plasma regions. In this case, higher $u_\perp$ values are found in *region_1* as compared with *region_2*. These $u_\perp$ profiles are shown in figure 10.a. The two data sets in this case are closer to each other than in the standard magnetic configuration (shown in figure 9.a), and as in the standard configuration, no clear trend is found in the $u_\perp$ vs. $k_\perp$ representation shown in figure 10.b.

In the third scenario described in section 3.1.1: higher collisionality plasmas ($n_e = 1.2 \times 10^{19}$ m^{-3}) heated with lower ECH power ($P_{ECH} = 250$ kW) deposited off-axis at $\rho_{ECH} = 0.4$, a different behaviour as regards $u_\perp$ has been encountered. Negative $u_\perp$ values are measured in the radial range $\rho \sim 0.6 - 0.9$ at turbulence scales $k_\perp \sim 3 - 12$ cm^{-1}. Contrary to the behavior found in the first scenario and in the configuration with high rotation transform, under these conditions a pronounced dependence of $u_\perp$ on $k_\perp$ is found that produces a high dispersion of the data when

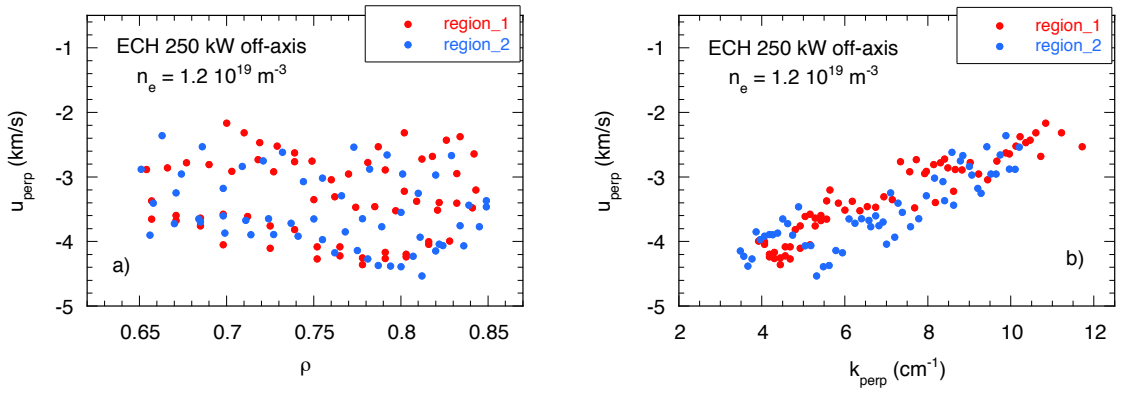

Figure 11. $u_\perp$ measured by the DR in the two plasma regions poloidally separated (*region_1* in red and *region_2* in blue) in the high collisionality plasmas, as a function of ρ (a) and $k_\perp$ (b). $P_{ECH} = 250$ kW off-axis at $\rho \sim 0.4$, $n_e = 1.2\ 10^{19}$ m^{-3}, standard magnetic configuration..

represented as a function of the plasma radius. Figure 11 shows this result. Velocities in the range from -2 to -4.5 km/s are measured without a clear radial dependence (figure 11.a) and scaling almost linearly with the turbulence wavenumber (figure 11.b). No differences are found when comparing the two poloidal plasma regions. As $v_{E\times B}$ does not depend on the turbulence wavenumber, this result indicates a non-negligible role of the intrinsic phase velocity of the turbulence v_{ph} on the total perpendicular rotation velocity $u_\perp$. It is worth mentioning that in TJ−II such a dependence of $u_\perp$ on $k_\perp$ has been observed so far only in these high collisionality ECH plasmas. Changes in the turbulence propagation properties with plasma collisionality have been also observed in Tore Supra [39]: at high collisionality, a dependence of $u_\perp$ on $k_\perp$ is measured that is absent in low collisionality plasmas. In both devices, $|u_\perp|$ decreases with increasing $k_\perp$. Changes in the phase velocity of the plasma turbulence have been also reported in AUG associated to the transition region between ITG and TEM instabilities [40]. As it is discussed in Refs. [39, 40], this type of measurements can be used to evaluate the form of the dispersion relation, which can then be compared with theoretical predictions from gyrokinetic simulations.

4. Discussion

The DR at TJ−II is a largely optimized system able to detect the back-scattered signal with a very high signal to noise ratio, thus the errors associated to the Gaussian fitting of the Doppler shifted spectra are considerably small [41]. The main error source is related to the power calibration used to compare the fluctuation level measured at different probing frequencies of the reflectometer. Each wavenumber spectrum is a combination of turbulence levels measured using a large set of probing frequencies and the spread of the data can be considered as the error in the measurement. Besides, the configuration of the DR hardware was fixed during the whole experimental campaign and the same

power calibration factors are applicable, thus, fluctuation levels measured at different scenarios can be directtly compared.

It is generally assumed that DR can provide accurate measurements of the $k_\perp$ turbulence spectra. However, there are some instrumental effects that should be taken into account. It is well known the transition from linear to saturated scattering regimes, predicted by the Doppler reflectometry theory [42] and found in the full-wave simulations [43,44], that would produce a saturation in the spectra at low $k_\perp$ due to the higher turbulence level at these scales. In addition, a non-linear regime has been recently described that can give rise to an enhanced backscattered power at high $k_\perp$ [45]. This enhanced power response would produce a flattening of the wavenumber spectrum at large $k_\perp$. Some experimental indications of this flattening have been recently reported as measured in the tokamak AUG [46]. In the simulations, the non-linear regime shows up at lower turbulence levels as compared to that for the saturated regime. Thus, as explained in Ref. [45], the signal at large $k_\perp$ may be enhanced by the non-linear response overestimating the spectral density, while the signal at small $k_\perp$ can still be linear and give an accurate measurement of the spectrum. These instrumental effects may be present in the wavenumber spectra discussed in section 3.1, however they could hardly explain the reported poloidal asymmetries. Complete saturation is not observed in the reported scenarios, although small, the spectral index is still finite (α_1 in figures 3−7). The low spectral indices measured at low $k_\perp$ can be consequence of being close to the saturation regime, but if this is the case, then one should conclude that the differences between the true wavenumber spectra at low $k_\perp$ should be more pronounced than that measured by the DR. Regarding the enhanced power response in the non-linear regime, it would produce an increase in the power response at high $k_\perp$ more pronounced in the poloidal region with stronger turbulence. This is clearly observed only in the spectra measured at $\rho = 0.71 \pm 0.05$ in the magnetic configuration with high rotational transform (figure 6.b). In this particular case, the measured asymmetry at high $k_\perp$ may be overestimating the real one. In the other scenarios, the spectral decay is more pronounced in *region_1* where the turbulence level is stronger, and the differences in the wavenumber spectra measured at the two poloidal regions are more pronounced at the intermediate $k_\perp$ range rather than at high $k_\perp$, what cannot be explained based on these instrumental effects.

Poloidal asymmetries in the turbulence have been studied in tokamaks, in the plasma scrape off layer showing a ballooning character [47], however very few measurements exist in the plasma bulk. Similarly, in stellarators, despite the turbulence asymmetries predicted by gyrokinetic simulations, the experimental results are scarce. In this sense, the systematic comparison of $k_\perp$ spectra measured at separate poloidal positions presented in this work can be considered as the first of a kind.

Regarding the measurements of the perpendicular rotation velocity of the plasma turbulence, DR theory [42] and simulations [43, 44] have demonstrated that the effects related to high turbulence levels do not affect the $u_\perp$ measurements. $u_\perp$ can be measured with high accuracy provided the DR diagnostic is properly optimized [41, 48]. Poloidal

asymmetries in $u_\perp$ have been reported in the tokamaks Tore Supra [49] and Textor [50]. In those cases $u_\perp$ profiles are measured in the low field side and at the top of the plasma. Faster propagation velocities are measured in the low field side in a broad range of plasma scenarios that the authors relate with the ballooned structure of the turbulence. The poloidal asymmetries in $u_\perp$ reported in this work as well as the $u_\perp$ dependence on $k_\perp$ found under specific plasma conditions are presently being the trigger for new theoretical simulation studies.

5. Summary

A systematic comparison of turbulence wavenumber spectrum and perpendicular rotation velocity measured using Doppler reflectometry at poloidally separated positions in the same flux-surface, has been carried out in the stellarator TJ-II.

Poloidal asymmetries in the $k_\perp$ spectrum are found that depend on plasma density, heating conditions and magnetic configuration. In the standard magnetic configuration, the strongest poloidal asymmetry is found in plasma scenarios with high electron temperature gradients at the plasma edge. This asymmetry reverses in the magnetic configuration with high rotational transform. The influence of the isotope mass has been also studied in ECH, as well as in NBI, Hydrogen and Deuterium dominated plasmas. No differences in the turbulence $k_\perp$ spectrum have been found associated to the ion mass. These results are in good qualitative agreement with the spatial localization of instabilities as calculated using the global gyrokinetic code EUTERPE in TJ-II plasmas [6, 31].

The most pronounced poloidal asymmetries in $u_\perp$ are found in low density plasmas in the neoclassical electron root confinement regime, in both Hydrogen and Deuterium plasmas, in the standard magnetic configuration. Similar values of $u_\perp$ are found in the magnetic configuration with high rotational transform however, as for the turbulence spectrum, the asymmetry in $u_\perp$ reverses. The asymmetry in the $u_\perp$ profile can be explained to be due to the radial dependence of electrostatic potential varying over the flux surface [37].

A non-negligible role of the intrinsic phase velocity of the turbulence v_{ph} on the total perpendicular rotation velocity $u_\perp$ is found in high collisionality ECH plasmas. The dependence of $u_\perp$ on $k_\perp$ can be used to evaluate the form of the dispersion relation, which can then be compared with theoretical predictions from gyrokinetic simulations.

Acknowledgments

The authors acknowledge the entire TJ-II team for their support. This work has been partially funded by the Spanish Ministry of Science and Innovation under contract numbers FIS2017-88892-P and ENE2015-70142-P. This work has been carried out within the framework of the EUROfusion Consortium and has received funding from the Euratom research and training programme 2014-2018 under grant agreement No 633053.

The views and opinions expressed herein do not necessarily reflect those of the European Commission

References

[1] A. Dinklage *et al.*, Nucl. Fusion **53**, 063022 (2013).
[2] M. Nadeem, T. Rafiq, and M. Persson, Physics of Plasmas **8**, 4375 (2001).
[3] V. Kornilov *et al.*, Physics of Plasmas **11**, 3196 (2004).
[4] P. Xanthopoulos, G. G. Plunk, A. Zocco, and P. Helander, Phys. Rev. X **6**, 021033 (2016).
[5] E. Sánchez, (43rd EPS Conference on Plasma Physics, Leuven, Belgium, 2016).
[6] E. Sánchez, (21st International Stellarator/Heliotron Workshop, Kyoto, Japan, 2017).
[7] D. D. Ho and R. M. Kulsrud, The Physics of Fluids **30**, 442 (1987).
[8] I. Calvo *et al.*, J. Plasma Physics **84**, 905840407 (2018).
[9] M. A. Pedrosa *et al.*, Nuclear Fusion **55**, 052001 (2015).
[10] J. M. García-Regaña *et al.*, Plasma Physics and Controlled Fusion **55**, 074008 (2013).
[11] J. M. García-Regaña *et al.*, Nuclear Fusion **57**, 056004 (2017).
[12] I. Calvo *et al.*, Nuclear Fusion **58**, 124005 (2018).
[13] M. Hirsch *et al.*, Plasma Physics and Controlled Fusion **43**, 1641 (2001).
[14] P. Hennequin *et al.*, Rev. Sci. Instrum. **75**, 3881 (2004).
[15] G. D. Conway *et al.*, Plasma Physics and Controlled Fusion **46**, 951 (2004).
[16] T. Happel *et al.*, Rev. Sci. Instrum. **80**, 073502 (2009).
[17] T. Estrada *et al.*, Plasma Phys. Control. Fusion **51**, 124015 (2009).
[18] T. Happel *et al.*, Phys. Plasmas **18**, 102302 (2011).
[19] A. Fernandez, W. Kasparev, and K. Likin, International Journal of Infrared and Millimeter Waves **22**, 649 (2001).
[20] M. Liniers *et al.*, Fusion Engineering and Design **123**, 259 (2017).
[21] F. Castejón, Á. Cappa, M. Tereshchenko, and Á. Fernández, Nuclear Fusion **48**, 075011 (2008).
[22] M. Hirsch *et al.*, Plasma Phys. Control. Fusion **48**, S155 (2006).
[23] B. van Milligen *et al.*, Rev. Sci. Instrum. **82**, 073503 (2011).
[24] J. Herranz *et al.*, Phys. Rev. Lett. **85**, 4715 (2000).
[25] T. Estrada *et al.*, Plasma Phys. Control. Fusion **43**, 1535 (2001).
[26] A. Hidalgo, D. Tafalla, B. Branas, and F. L. Tabares, Rev. Sci. Instrum. **75**, 3478 (2004).
[27] E. de la Luna, J. Sánchez, V. Tribaldos, and T. Estrada, Rev. Sci. Instrum. **72**, 379 (2001).
[28] J. Fontdecaba *et al.*, Fusion Sci. Technol. **46**, 271 (2004).
[29] J. Arévalo, J. Alonso, K. McCarthy, and J. Velasco, Nuclear Fusion **53**, 023003 (2013).
[30] G. Jost *et al.*, Physics of Plasmas **8**, 3321 (2001).
[31] E. Sánchez *et al.*, (27th IAEA FEC, EX/P1-11, Ahmedabad, India, 2018).
[32] U. Losada *et al.*, Plasma Physics and Controlled Fusion **60**, 074002 (2018).
[33] M. G. Shats, H. Xia, and H. Punzmann, Phys. Rev. E **71**, 046409 (2005).
[34] L. Guimarais *et al.*, Plasma and Fusion Research **3**, S1057 (2008).
[35] T. Happel, T. Estrada, and C. Hidalgo, Eur. Phys. Lett. **84**, 65001 (2008).
[36] J. L. Velasco *et al.*, Plasma Physics and Controlled Fusion **55**, 124044 (2013).
[37] J. M. García-Regaña *et al.*, Plasma Physics and Controlled Fusion **60**, 104002 (2018).
[38] J. L. Velasco *et al.*, Plasma Physics and Controlled Fusion **60**, 074004 (2018).
[39] L. Vermare *et al.*, Phys. Plasmas **18**, 012306 (2011).
[40] T. Happel *et al.*, Phys. Plasmas **22**, 032503 (2015).
[41] T. Happel, E. Blanco, and T. Estrada, Rev. Sci. Instrum. **81**, 10D901 (2010).
[42] E. Z. Gusakov, A. V. Surkov, and A. Y. Popov, Plasma Physics and Controlled Fusion **47**, 959 (2005).
[43] E. Blanco and T. Estrada, Plasma Physics and Controlled Fusion **50**, 095011 (2008).
[44] C. Lechte, IEEE Trans. Plasma Sc. **37**, 1099 (2009).

[45] J. R. Pinzon *et al.*, Plasma Physics and Controlled Fusion **59**, 035005 (2017).
[46] T. Happel *et al.*, Plasma Physics and Controlled Fusion **59**, 054009 (2017).
[47] J. A. Boedo, Journal of Nuclear Materials **390**, 29 (2009).
[48] M. Hirsch and E. Holzhauer, Plasma Physics and Controlled Fusion **46**, 593 (2004).
[49] L. Vermare *et al.*, Physics of Plasmas **25**, 020704 (2018).
[50] A. Krämer-Flecken, Y. Xu, S. Zoletnik, and T. Team, *Poloidal rotation asymmetry and relation to turbulence* (In Proceedings of the 39th EPS Conference and 16th International Congress on Plasma Physics, Stockholm, Sweden, 2012), Vol. 36F, p. P5.044.